Photochromic Thermoelectric Smart Window for Season-Adaptive Solar Heat and Daylight Management

Meng, Weihao; Kragt, Augustinus J.J.; Hu, Xiaowen; van der Burgt, Julia S.; Schenning, Albertus P.H.J.; Yue, Yuchen; Zhou, Guofu; Li, Yong; Wang, Jingxia; More Authors

DOI
10.1002/adfm.202402494

Publication date
2024

Document Version
Final published version

Published in
Advanced Functional Materials

ADVANCED FUNCTIONAL MATERIALS
www.afm-journal.de

Photochromic Thermoelectric Smart Window for Season-Adaptive Solar Heat and Daylight Management

Weihao Meng, Augustinus J.J. Kragt, Xiaowen Hu, Julia S. van der Burgt, Albertus P.H.J. Schenning, Yuchen Yue, Guofu Zhou, Laifeng Li, Ping Wei, Wenyu Zhao, Yong Li, Jingxia Wang,* and Lei Jiang*

Photochromic smart windows have drawn increasing attention as an approach to improve building energy efficiency and enhance indoor daylight comfort. However, existing photochromic smart windows still block sunlight from entering the room on sunny winter days, causing additional energy consumption for heating. Herein, a dual-mode smart window is designed with decoupled photo and thermal functions by combining colorless Fe-doped WO_3 photochromic film with window rotation. Based on this, selective heating and cooling of the room between winter and summer is achieved while maintaining the daylight comfort benefits during all seasons. As a proof of concept, the smart window reduces the temperature of a model house by up to 7.9 °C in summer mode, while in winter mode the temperature is only reduced by 0.7 °C. The proposed seasonally adaptive dual-mode smart window obtains by window rotation overcomes the limitations of conventional photochromic smart windows, which not only achieves better energy efficiency but also retains improved daylight comfort. Furthermore, it demonstrates that the heat absorbed by the smart window can be harnessed to produce electricity through the integration of thermoelectric modules within the glazing, which enhances its impact on reducing energy consumption.

1. Introduction

Dramatic global climate change, represented by the 2023 global heat waves, warns us of the urgent need for energy efficiency and reduction of CO_2 emissions. Buildings account for ≈34% of global energy consumption and 37% of energy-related CO_2 emissions in 2022.[1] Among this, 50% of building energy consumption is spent on building heating, ventilation, and air-conditioning systems, highlighting the significant demand for temperature control in building spaces.[2–4] In particular, heat transfer through the building envelope has been reported to account for more than 50% of the total building thermal load. Therefore, the improvement of energy efficiency of the building envelope is crucial for achieving energy savings and reducing emissions.[5] Windows are considered to be the least energy-efficient component of a building's envelope due to heat loss in winter and solar heat gain in summer.[6] Current approaches to this challenge include: 1) Inhibiting the energy exchange between indoor and outdoor by insulating thermal conduction, convection, and radiation of windows, which is achieved by using gas-filled, aerogel[7,8] double glazing and Low-E glass; 2) Dynamically modulating emittance or transmittance of windows under external triggers to accommodate the heating/cooling needs of the buildings in different seasons. The triggers for the system can be human energy inputs, including mechanical (stretching[3,9] or flipping[10]) and electrical[11–14] action or changes in the environment, such as temperature (thermochromic)[15–24] and light intensity (photochromic).[25–29]

W. Meng, Y. Yue, J. Wang, L. Jiang
CAS Key Laboratory of Bio-inspired Materials and Interfaces Sciences
Technical Institute of Physics and Chemistry
Chinese Academy of Sciences
Beijing 100190, China
E-mail: jingxiawang@mail.ipc.ac.cn

W. Meng, L. Li, J. Wang
Center of Material Science and Optoelectronics Engineering
School of Future Technologies
University of Chinese Academy of Sciences
Beijing 101407, China

A. J. Kragt, A. P. Schenning
Laboratory of Stimuli-responsive Functional Materials & Devices
Department of Chemical Engineering and Chemistry
Eindhoven University of Technology
P.O. Box 513, Eindhoven 5600 MB, The Netherlands

A. J. Kragt
Department of Architecture and the Built Environment
Delft University of Technology
Julianalaan 134, Delft 2628 BL, The Netherlands

A. J. Kragt, J. S. van der Burgt, G. Zhou
ClimAd B.V. Technology
Valkenaerhof 68, Nijmegen 6538 TE, The Netherlands

The ORCID identification number(s) for the author(s) of this article can be found under https://doi.org/10.1002/adfm.202402494

DOI: 10.1002/adfm.202402494

Thermochromic and photochromic (PC) smart windows are considered to be a better choice than mechanically or electrically driven smart windows due to their structural simplicity, passive light modulation, and zero energy input. Thermochromic and photochromic smart windows modulate the energy flux of solar radiation through windows by improving either their absorbance or scattering. Smart windows with tunable scattering including hydrogels,[17–20] ionic liquid gels,[21,22] and liquid crystals[23] offer advantages in transparency and solar modulation. However, their scattering affects the field of view and people's observation of the outdoors. Smart windows made of materials such as VO_2,[15,16] perovskite,[24] and WO_3[25–29] can adjust their sunlight absorption, while still remaining see-through. However, most of the current research focuses on the direct transmittance of sunlight (T_{sol}) and ignores the solar heat absorbed by the window. The transfer of this heat into the room can lead to an increase in the room temperature, reducing the energy efficiency of smart windows in summer. However, this part of energy can also be captured and used, for example, to heat up the room in winter or to generate electricity through thermoelectric conversion.[30]

Beyond heating, windows also need to provide sufficient total interior illumination while limiting excessive brightness and localized glare.[31] PC smart windows have sufficient advantages in this respect because the trigger for photochromism is the intensity of sunlight. At high solar intensities, PC smart windows will be in their tinted state, preventing excessive brightness and glare in the room, while at low solar intensities, they will be transparent and maximize daylight entrance. However, in terms of energy efficiency PC smart windows are not the optimal choice in countries with more variable weather conditions throughout the seasons. Although they can provide more annual energy savings compared to non-adaptive solar control systems, they will induce an additional energy use for heating in winter, as on sunny winter days the tinted state will also block solar heat.[32] Window rotation technology is a simple and effective approach to accommodate the thermal management needs of building interiors in different seasons and has been extensively investigated for dynamic building envelopes.[33–37]

Here, a dual-mode smart window with decoupled photo and thermal functions is achieved by combining photochromic film technology with mechanical window rotation, which improves the energy efficiency of photochromic smart windows in winter, while maintaining the daylight comfort benefits through all seasons. The summer mode of the smart window can modulate the visible light entering the room to increase daylight comfort. It also can reduce the solar heat entering the room to lower the indoor temperature, which will reduce the energy consumption required for cooling. The winter mode of the smart window not only modulates the visible light but also allows solar heat to enter the room even when tinted, which avoids additional energy consumption for space heating. As a result, in climates with significant seasonal variations, the use of dual-mode photochromic smart windows can increase energy savings by up to five times compared to using the summer mode alone. In addition, this work shows the possibility of generating electricity by utilizing the heat absorbed by the photochromic film.

2. Results and Discussion

2.1. Preparation and Photochromic Process of the PC Film

For an ideal PC smart window, a high solar modulation and a fast and reversible switching speed are desired. In our previous work, we developed copper-doped tungsten trioxide (WO_3) and polymethyl methacrylate (PMMA) composite photochromic (Cu-W-PC) films.[32] The copper doping was effective in accelerating the bleaching process, that is, the recovery of the PC film from the tinted to the transparent state. However, the introduction of copper ions resulted in a yellowish color of the prepared films in the transparent state, which is unfavorable for a window application. Here, we tried different metal ion doping (Figure 1A) to accelerate the bleaching process without causing color distortions (Figure S1, Supporting Information) using our blade-coating method. It was found that the Fe-doped WO_3-PMMA photochromic (Fe-W-PC) films were able to meet the requirements for both color neutrality and accelerated bleaching. The Fe-W-PC films are in the transparent state immediately after preparation, whereas the other ion-doped W-PC films exhibit a tinted state after preparation, indicating that they do not oxidize the W-ions to the desired oxidation (W^{6+}) state (Figure S1, Supporting Information). In addition, the transmittance spectra of different ion-doped W-PC films show scattering in the visible region, indicating a too large WO_3 particle size, whereas the Fe-W-PC film shows a high color-neutral transparency in the transparent state. Photographs of the Fe-doped W-PC films with different concentrations all show rapid and uniform tinting when irradiated with a solar lamp (Figure S2, Supporting Information), and the fastest bleaching rate is observed with 40 mol% (relative to W) Fe doping (Figure S3, Supporting Information). Therefore, unless otherwise stated, all subsequent Fe-W-PC films will be prepared with 40 mol% Fe doping.

The prepared Fe-W-PC film exhibited a colorless and transparent state when not exposed to sunlight. After sunlight exposure, it uniformly turned to a blue tinted state (Figure 1B). The uniform color change is achieved due to the consistent thickness (≈50 μm) of the Fe-W-PC film and the homogeneous distribution of WO_3 nanoparticles (with a mean size of 8.5 nm) are the basis for achieving a uniform color change. This can be observed in the scanning electron microscopy (SEM) pictures in top- and cross-view and the corresponding energy dispersive spectrometer

X. Hu, G. Zhou
Guangdong Provincial Key Laboratory of Optical Information Materials and Technology
Institute of Electronic Paper Displays
South China Academy of Advanced Optoelectronics
South China Normal University
Guangzhou 510006, China
P. Wei, W. Zhao
State Key Laboratory of Advanced Technology for Materials Synthesis and Processing
Wuhan University of Technology
Wuhan 430070, China
Y. Li
CAS Key Laboratory of Cryogenics
Technical Institute of Physics and Chemistry
Chinese Academy of Sciences
Beijing 100190, China
E-mail: liyong1897@mail.ipc.ac.cn

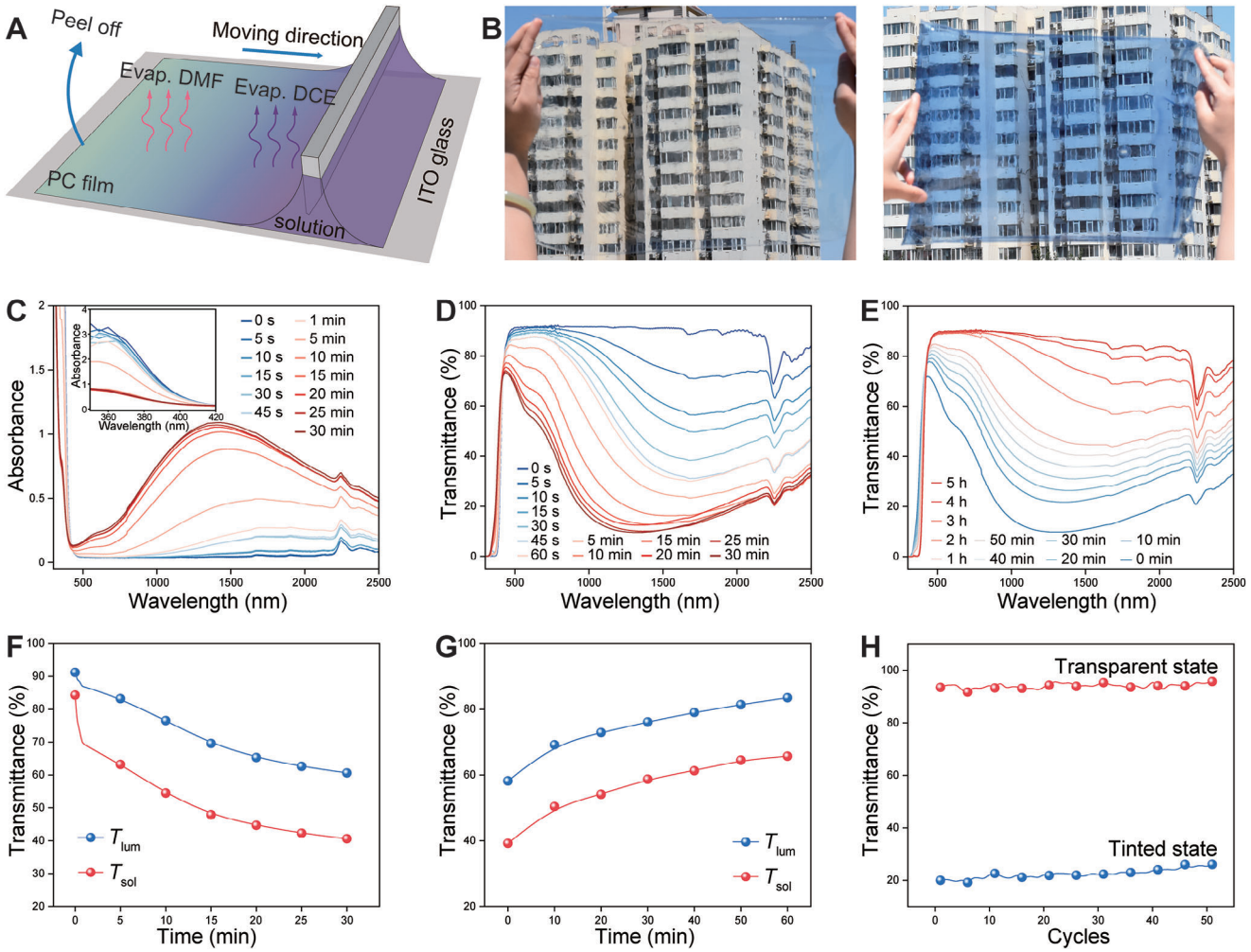

Figure 1. Preparation and working principle of Fe-W-PC film. A) Schematic depiction of the blade coating fabrication process for the Fe-W-PC film: $FeCl_3$/WCl_6/N,N-dimethylformamide.(DMF) solution and PMMA/1,2-Dichloroethane (DCE) solution were thoroughly mixed and then blade-coated and dried to form a film. B) Photos of Fe-W-PC film in transparent state (left) and tinted state (right). C,D) Absorbance (C) and transmittance (D) spectra of the Fe-W-PC film during the tinting (irradiation with solar light, 100 mW cm^{-2}). E) Transmittance spectra of the Fe-W-PC film during the bleaching process. F,G) T_{lum} and T_{sol} changes of the Fe-W-PC film during the (F) tinting and (G) bleaching process. H) Transmittance changes of the Fe-W-PC films at 1050 nm during more than 50 cycles of tinting and bleaching.

(EDS) mapping (Figure S4, Supporting Information). The high transparency of the Fe-W-PC film is due to the small particle size of the WO_3 nanoparticles, as observed by the Aberration-Corrected High-Angle Annular Dark-Field Scanning Transmission Electron Microscopy (HAADF-STEM) photographs (Figure S5, Supporting Information). This small particle size and high dispersion of WO_3 is achieved through the proposed limiting effect[32] of PMMA during the in situ growth of WO_3 in PMMA (Figure S6, Supporting Information). The additional absorption peak resulting from Fe doping is located at 360 nm (inserted Figure 1C), while the corresponding absorption peak for Cu doping is located at 400 nm.[32] Therefore, the Fe-W-PC film appears colorless whereas the Cu-W-PC film appears yellowish. The Fe-W-PC film has a great UV shielding effect due to the absorption of UV light caused by WO_3 and Fe doping. This can effectively reduce the intensity of UV light entering the room (Figure S7, Supporting Information). The photochromic effect of the Fe-W-PC film was further explored by irradiation with a solar spectrum mimicking lamp (100 mW cm^{-2}), which demonstrated changes in absorbance (Figure 1C) and transmission over time (Figure 1D). As the irradiation time increases, the Fe-W-PC film gradually absorbs more light in the visible and near-infrared range, resulting in a blue tint. This tint is caused by the valence change of W (from W^{6+} to W^{5+}). At the same time, the absorption at 360 nm gradually decreased, which is derived from the valence change of Fe. The increase in absorption leads to a decrease in the transmittance. During the initial stage of tinting (within 1 min of irradiation time), there is a significant decrease in transmittance of the near-infrared range, without significant change in the visible range (T_{lum}). The transmittance change in the near-infrared band (1100–2500 nm) mainly originates from the localized surface plasmon resonance (LSPR) mechanism. This mechanism arises from the collective oscillations exhibited by the sufficient photogenerated electrons injected into the conduction band of

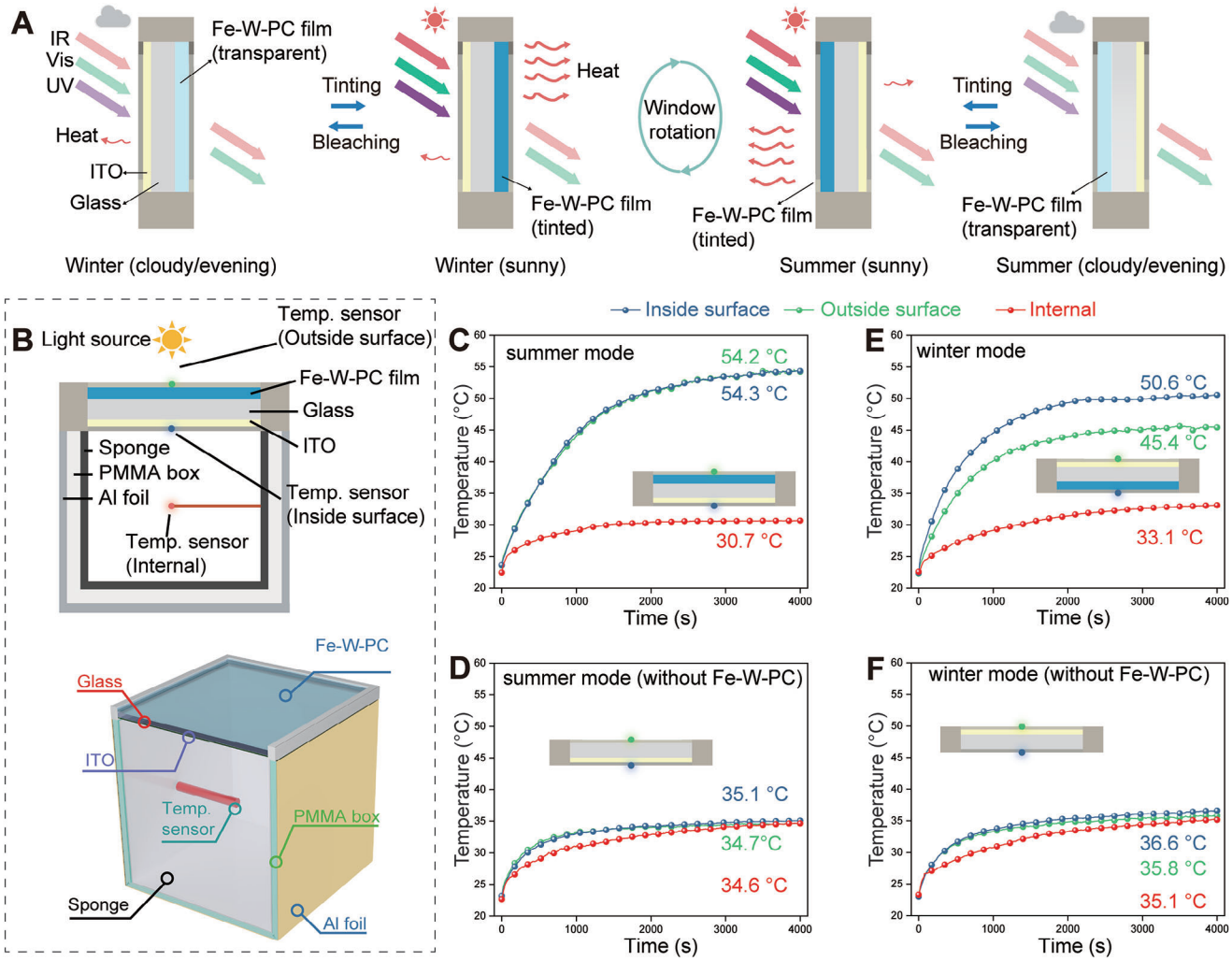

Figure 2. The design of the SDP smart windows and the effect on indoor temperature. A) Design and working principles of the SDP window. B) Schematic representation of the model house with the SDP window. C–F) Temperature curves for the model houses with the SDP windows in (C)summer mode, (D) summer mode without Fe-W-PC film, (E) winter mode, and (F) winter mode without Fe-W-PC film under the simulated sunlight 100 mW cm^{-2} for 4000 s.

WO_3.[38–39] As the irradiation continues, the transmittance in the visible range decreases significantly. The decrease is primarily caused by the transfer of electrons between tungsten ions with different valence states, that is, the small polariton hopping between two unequal tungsten ions (W^{6+} and W^{5+}).[40] After 30 min of irradiation, Fe-W-PC is fully tinted, resulting in a transmittance decrease across the visible and near-infrared parts of sunlight, ranging from 400 to 2500 nm. The tinted Fe-W-PC film gradually bleaches and returns to its original transparent state in the absence of sunlight irradiation. This causes a gradual increase in its transmittance(Figure 1E). During the tinting process, T_{lum} decreased from 91% to 60%, and solar transmittance (T_{sol}) decreased from 84% to 40% (Figure 1F). After ≈1 h of bleaching, T_{lum} is fully recovers (Figure 1G). However, this process takes ≈5 h in the near-infrared part (Figure 1E). Furthermore, the tinting and bleaching processes of the Fe-W-PC films exhibited excellent cycling stability, without significant changes in the spectra after 50 cycles (Figure 1H). The Fe-W-PC film is also highly flexible with a tensile strength of 38.5 MPa, making it suitable for direct application to glass (Figure S8, Supporting Information). As smart windows are frequently used in outdoor environments for extended periods, we tested the contact angle of the Fe-W-PC film. It was 72.5° in the tinted state and 65.0° in the transparent state (Figure S9, Supporting Information).

2.2. Dual-Mode Photochromic Smart Window

Inspired by the rotation technology for dynamic thermal management of building envelopes, we designed an asymmetric structure for single glazed dual-mode photochromic (SDP) window with seasonal adaptability. The structure consists of low-emissivity indium tin oxide (ITO glass) and Fe-W-PC film (Figure 2A). The orientation of the Fe-W-PC film and ITO glass can be changed by rotation, allowing for switching between winter and summer modes of the SDP window. Due to the

UV-absorbing effect of the ITO glass (Figure S10, Supporting Information), the photochromic effect of the SDP window in winter mode is slightly suppressed (Figure S11, Supporting Information). However, it still adequately modulates the sunlight entering the room to improve the daylight comfort. During winter, the ITO layer with low emissivity faces the outdoors to limit the radiation heat loss, while the Fe-W-PC film with high emissivity faces the indoors to transfer the absorbed heat to the interior of the room. During summer, the SDP window should be rotated so that the Fe-W-PC film faces outside. This allows the photochromic effect of the Fe-W-PC film to automatically modulate the solar heat and daylight entering the room, which is helpful in reducing the energy consumption required for indoor cooling and improving the daylight comfort. Simultaneously, the high emissivity of the Fe-W-PC film allows heat transfer to the outside, while the low emissivity of the ITO layer reduces the heat absorbed by the Fe-W-PC film to be radiated to the inside of the room (Figure S12, Supporting Information).

Model tests were conducted to investigate the energy-saving performance of the SDP smart window as a proof of concept (Figure 2B). A $15 \times 15 \times 15$ cm^3 box was used as a model, and the air temperature inside the box as well as the temperature of the inside and outside surfaces of the SDP window were recorded during irradiation with a solar lamp (100 mW cm^{-2}) for analysis (Figure 2C–F). In the summer mode of the SDP window, the temperature inside the box (Figure 2C) was 3.9 °C lower than that without Fe-W-PC film (Figure 2D), while in the winter mode, the temperature inside the box (Figure 2E) was only 2 °C lower than the case without Fe-W-PC film (Figure 2F). This demonstrates that SDP smart windows can reduce the indoor temperature in the summer and suppress this cooling effect in the winter. In summer mode, the temperature on the inside and outside surfaces of the SDP window both reached ≈54 °C, much higher than the indoor temperature, which comes from the absorption of sunlight by the tinted Fe-W-PC film. Although the ITO glass with low emissivity on the inside surface suppresses heat radiation to the interior, high temperature of the inside surface still results in heat transfer and heat convection into the interior of the room, leading to an increase in room temperature and consequently, an increase in cooling energy consumption. In winter mode, surface temperatures of both the inside and outside of the SDP windows are lower compared to the summer mode. This is due to the photochromism of the Fe-W-PC film being somewhat suppressed, resulting in less heat absorption. However, the higher outside surface temperature of the winter mode is still a concern, as it may lead to heat loss.

Considering the above thermal disadvantages of the SDP smart windows, we designed a dual-mode photochromic smart window, which combines commercial Low-E coated double glazing with the Fe-W-PC film (DDP window). The strategy for implementing the DDP window is similar to that of the SDP window, in that they are all catered for different seasons with a simple rotation (Figure 3A,B). In addition to having the same Low-E surface as the SDP window, the double-layer construction of the DDP window and the inert gas filling further reduces the energy exchange between its inside and outside surfaces, thus increasing its thermal insulation. The photochromism of DDP window allows T_{lum} to follow the outdoor light intensity in winter and summer, improving daylight comfort. The Fe-W-PC film retains its tint and solar heat absorption properties during the winter. However, due to the excellent insulation of DDP windows, this heat is mainly transferred to the interior of the room, effectively heating the room. During summer, the heat absorbed by the Fe-W-PC film is mainly transferred to the exterior, reducing the indoor temperature and the energy consumption required for indoor cooling. By combining photochromic technology with mechanical rotation, the designed DDP window achieves the decoupling of photo and thermal functions. This improves indoor daylight comfort in both winter and summer while providing beneficial thermal functionalities for both seasons.

Photos of DDP windows in winter and summer mode before (Figure 3C) and after photochromic (Figure 3D) show that after forming a DDP window with Low-E coated double glazing the Fe-W-PC film can still maintain a uniform tinting in sunlight. This ability is the basis for their capacity to modulate visible light entering the room and enhance indoor daylight comfort. Infrared photographs were taken of the inside and outside surfaces of the DDP windows in sunlight in winter and summer modes. The results showed significant temperature differences (Figure 3E,F). During the winter mode, the Fe-W-PC film on the inner surface increased the temperature by 40.8 °C after absorbing sunlight (Figure 3F), which is 4 °C higher than the outer surface temperature of 36.8 °C (Figure 3E). This facilitates heat transfer to the indoors. During the summer mode, the temperature of the inner surface of the DDP window is 33.5 °C, while the outer surface temperature is 48.8 °C. This temperature difference of 15.3 °C allows heat transfer to the outdoors.

The energy-saving effect of the DDP windows was verified using the same model (Figure S13, Supporting Information). In the winter mode of the DDP window without Fe-W-PC (Figure 4A), the air temperature inside the box reached 31.1 °C after irradiation. After equipping the window with Fe-W-PC film, the air temperature inside the box reached almost the same level (30.5 °C, Figure 4B). The Fe-W-PC film on the inside of the DDP window absorbs solar heat, which is then transferred more to the interior during the winter mode. However, the transfer of heat to the exterior is blocked by the Low-E-coated double windows. Due to the superior thermal resistance of the Low-E coated double window, the temperature difference between the air inside the box is just 0.6 °C. This is considerably lower than the temperature difference created by SDP windows (2 °C) under the same conditions. During the summer mode (Figure 4C), the temperature of the outside surface of the DDP windows reached as high as 55.5 °C, which is 22.8 °C higher than the inside surface (32.7 °C). This indicates that the heat absorbed by the Fe-W-PC film is blocked by the Low-E-coated glass pane. Consequently, the air temperature inside the box (27.8 °C) is 4.1 °C lower than the box with a DDP window without Fe-W-PC film (Figure 4D). Our view is confirmed by outdoor tests. The box equipped with the DDP window in summer mode reduced the maximum indoor temperature by 7.9 °C (Figure 4E) on a sunny summer day, as intended for this season. In contrast, the DDP window in winter mode did not reduce the indoor temperature. The maximum indoor temperature of the box equipped with the winter mode DDP window was only 0.3 °C lower than the window without Fe-W-PC film (Figure 4F) during a sunny winter day. However, using a DDP window in summer mode would reduce the indoor temperature by 3.9 °C, which is not desirable during the winter season. In summary, the

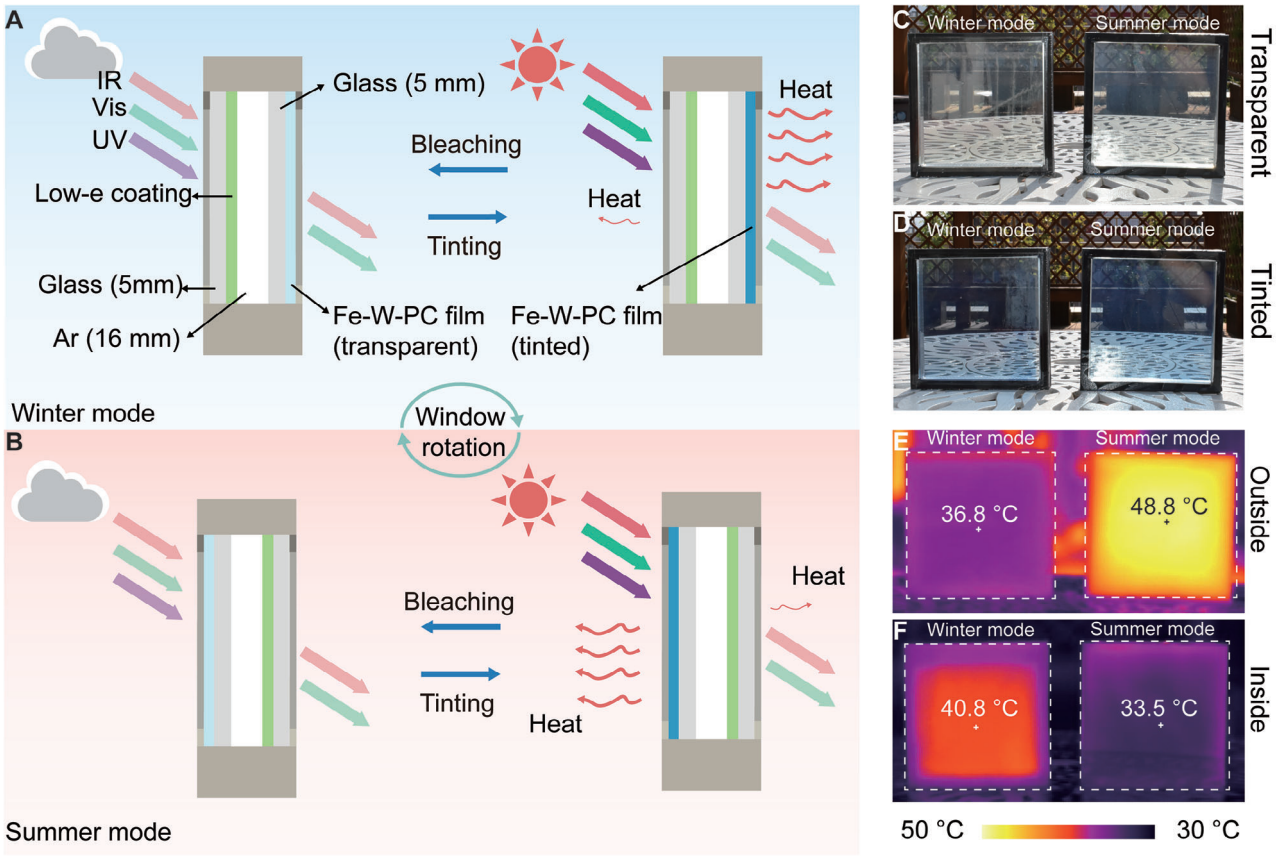

Figure 3. The design and working principles of the DDP smart window in A) winter mode and B) summer mode. Photos of the DDP window in C) transparent state and D) tinted state (right). Infrared photos of the E) outside and F) inside surfaces of the DDP windows in sunlight in winter mode and in summer mode.

rotation of the DDP window enables different modes for winter and summer, each with different heating effects on the room. The summer mode re-radiates less heat into the room than the winter mode.

In addition to regulating the heating by solar radiation for seasonal temperature control, the temperature difference between the inner and outer surfaces of the DDP window can be utilized to generate electricity through thermoelectric devices, as illustrated in Figure 5A. The thermoelectric device is placed between the two glass layers of the DDP window and distributed along its edges. The Fe-W-PC film continuously collects heat and conducts it laterally through the glass to the thermoelectric devices. The generation of electric current under direct sunlight irradiation was measured using a current multimeter. The thermoelectric devices in the DDP windows with Fe-W-PC film can deliver an output voltage of 54.6 mV (Figure 5B, left) by directly harvesting from the outdoor sunlight. In comparison, the output voltage is 37.1 mV without Fe-W-PC film (Figure 5B, right). The plots of current–voltage and current–power density under outdoor sunlight show the open-circuit voltage (80 mV) and the maximum power density (0.15 mW) for the DDP windows with Fe-W-PC film. These values are higher than those without Fe-W-PC film, which were 60 mV and 0.076 mW, respectively. This demonstrates the potential of energy harvesting through thermoelectric devices in DDP windows.

2.3. Energy-Saving Potential of DDP Windows

To demonstrate the energy-saving potential of the DDP windows, we used DesignBuilder to calculate the energy consumption of an office building equipped with DDP windows (Figure S14, Supporting Information). Steady-state optical properties are demonstrated for Fe-W-PC films attached to single glass panels at different sunlight intensities (Figure S15, Supporting Information), which were used to calculate the variation of visible light transmittance (T_{lum}) and solar heat gain coefficient (SHGC) of DMP windows with solar intensity in winter and summer mode (Figure 6A). The T_{lum} of the DDP window decreases with increasing sunlight intensity in both winter and summer modes, which is consistent with our design and indicates its ability to increase indoor daylight comfort. SHGC is a measure of the amount of solar radiation that enters a building through a window and is released as heat. It takes into account both the direct transmission of sunlight through the window, which is affected by the window's solar transmittance (T_{sol}), and the secondary heat transfer to the interior after the sunlight is absorbed by the window. The SHGC of the summer mode decreases significantly with increasing sunlight intensity, indicating that the amount of heat entering the room during summer can be adjusted adaptively according to the intensity of sunlight. In contrast, the SHGC of the winter mode varies little with the sunlight intensity. This is because the

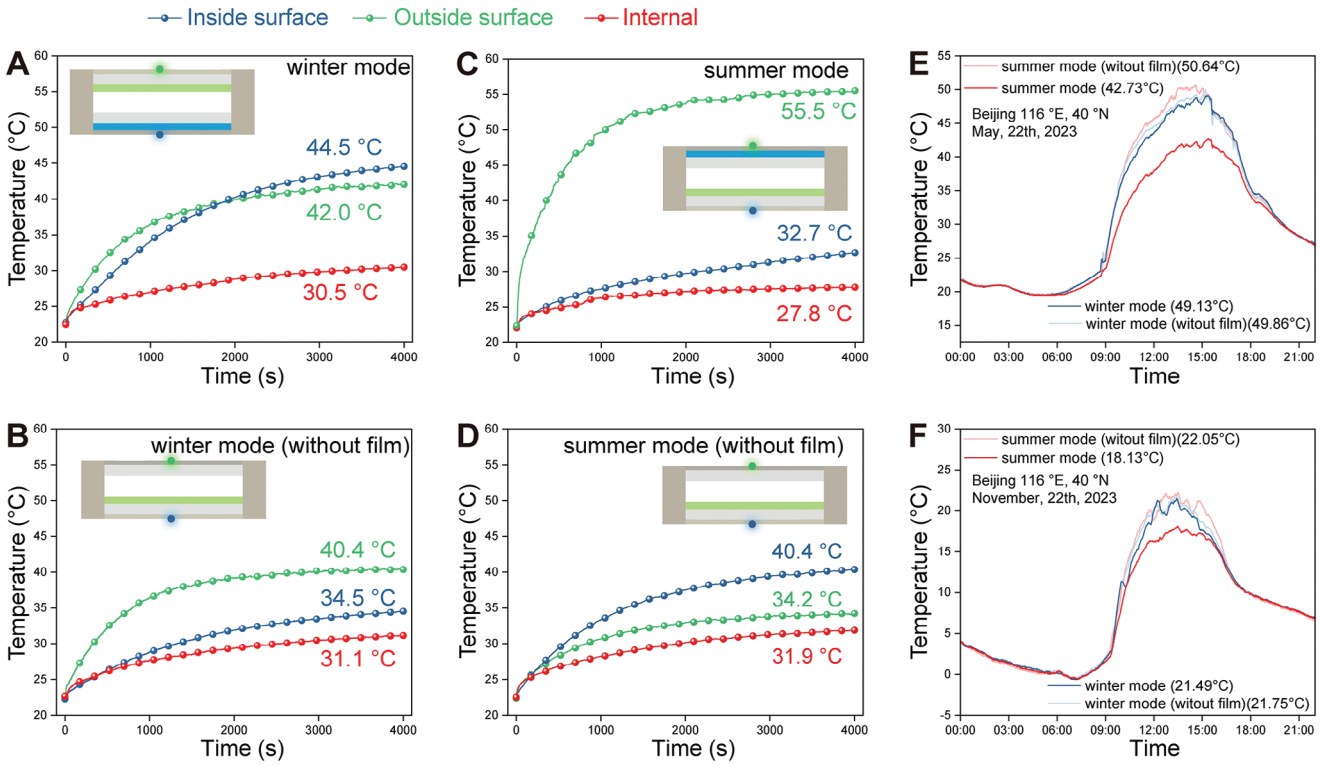

Figure 4. The effect of the DDP smart window on indoor temperature. A–D) Temperature curves for the model houses with the DDP windows in (A) winter mode, (B) winter mode without Fe-W-PC film, (C)summer mode, and (D) summer mode without Fe-W-PC film under the simulated sunlight 100 mW cm^{-2} for 4000 s. E,F) Temperature curves for the model houses with the DDP windows under field test for 1 sunny day in (E) summer and (F) winter mode.

heat absorbed by the Fe-W-PC film is mainly transferred inside the room, resulting in a relatively constant SHGC. The findings suggest that DDP windows can decrease the amount of solar heat entering a room during summer while having minimal impact during winter.

Based on the window characteristics at specific sunlight intensities we calculated the annual energy consumption on lighting, heating, and cooling of a model office equipped with the DDP windows in nine cities with different climates using DesignBuilder (Figure S16, Supporting Information). To assess the impact of the DDP windows, we also included calculations for energy consumption without the Fe-W-PC film (Figure 6B). The energy consumption of DDP windows in winter mode is minimally impacted compared to the case without Fe-W-PC films. This is because the DDP windows in winter mode have a consistent SHGC and do not reduce the solar heat entering the room. On the other hand, the use of the DDP windows in summer mode reduces energy consumption for cooling in all cities. Especially in warm regions, such as Johannesburg, it can be achieved energy savings of up to 50.6% per year. However, the energy saving benefits of the DDP windows in summer mode may not be as pronounced in areas with significant seasonal weather changes

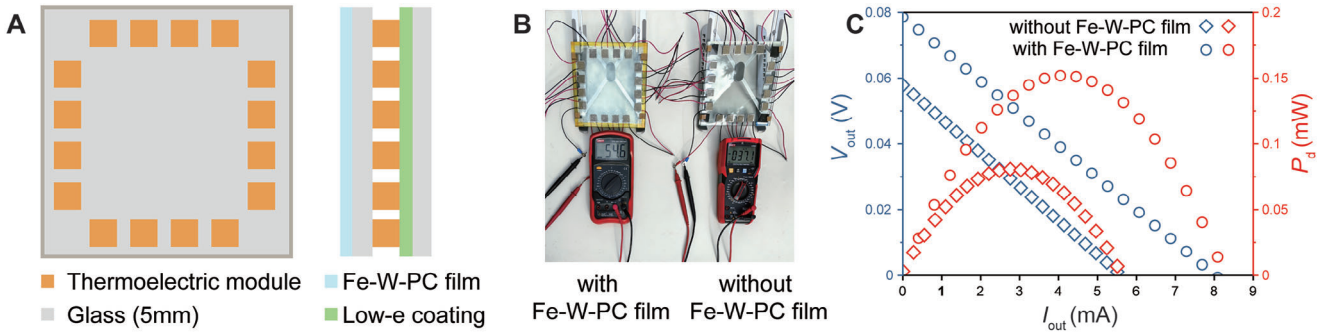

Figure 5. A) Schematic illustration of the architecture for the DDP window with thermoelectric devices. B,C) Proof-of-concept demonstration of the power-generating performance (B) and measured current–voltage and current–power density plots (C) of thermoelectric devices sandwiched between a typical DDP window with or without Fe-W-PC film.

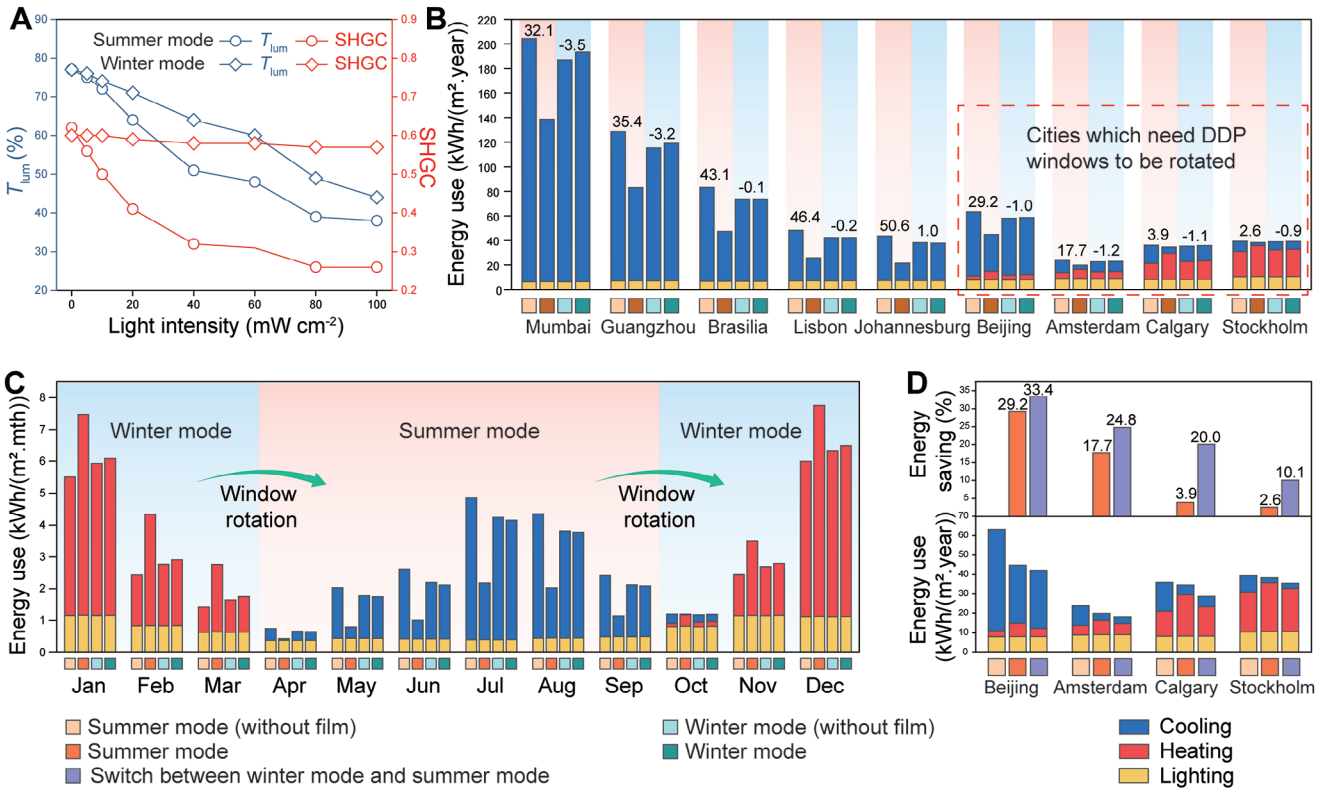

Figure 6. Simulation of the energy-saving performance of the DDP windows. A) Variation for T_{lum} and SHGC of the DDP windows in winter and summer mode under different light intensities. B) Calculated annual energy use of the model office equipped with the DDP window in different cities. The energy saving percentage of the DDP windows in summer and winter mode compared to the situations without Fe-W-PC film were put on top of the bars. C) Calculated monthly energy use of model office enveloped with the DDP window in Calgary. D) Calculated annual energy use and energy saving of the model office equipped with the DDP window in continuous summer mode and switching mode in Beijing, Amsterdam, Calgary, and Stockholm.

and high heating demands during winter. This is due to the fact that the DDP windows in summer mode also limit the amount of solar heat entering the room during colder weather, which can result in increased heating energy consumption. Therefore, in these cities, the DDP windows should be in summer mode when the building's energy is consumed primarily for interior cooling. In contrast in winter mode when the building's energy is consumed primarily for interior heating. In Calgary, for example (Figure 6C), the energy used for indoor heating accounts for the majority of energy consumption in January, February, March, October, November, and December. Therefore, the DDP windows in winter mode result in lower indoor energy consumption compared to summer mode. Conversely, for the remaining months, the indoor energy consumption is mainly due to cooling, making the energy-saving effect of the DDP windows in summer mode is more apparent. In summary, the rational switching of the DDP windows between winter and summer modes during the year can effectively improve the energy efficiency of buildings in areas with large seasonal weather changes (Figure 6D; Figure S17, Supporting Information). In Calgary, the model office equipped with the DDP windows saved only 3.9% of energy consumption in summer mode compared to the DDP windows without Fe-W-PC film. However, rotating the DDP window between summer and winter modes in April and October, respectively, resulted in a 20% of energy consumption reduction, which is more than a fivefold increase in energy savings. Similar results were observed in Beijing, Amsterdam, and Stockholm, the energy savings effect was also increased accordingly.

3. Conclusion

The as-prepared DDP smart windows exhibit seasonally adaptive solar thermal and light management properties, which realize decoupled photo and thermal functions under different seasons by the rotatable structure design. In summer mode, the DDP window not only improves the indoor daylight comfort by regulating the visible light entering the room (ΔT_{lum} = 39%) but also lowers the indoor temperature (7.9 °C) and reduces the energy consumption required for indoor cooling by reducing the solar heat gain ($\Delta SHGC = 0.36$) entering the room. In winter mode, however, the DDP windows do not block the solar heat from entering the room ($\Delta SHGC = 0.03$), resulting in a limited reduction of indoor temperature (0.7 °C) and minimal additional energy consumption for heating. Switching DDP windows between winter and summer modes can enhance the energy-saving potential of photochromic materials by up to five times in climates with high seasonal variability. In addition, the heat absorbed by the smart window can be used to generate electricity, increasing its application potential in the energy sector.

4. Experimental Section

Materials: Tungsten chloride (WCl_6), iron (III) chloride ($FeCl_3$), Platinum (IV) chloride ($PtCl_4$), tin (IV) chloride ($SnCl_4$), cobalt (II) chloride ($CoCl_2$), zinc (II) chloride ($ZnCl_2$), manganese (II) chloride ($MnCl_2$), bismuth (III) chloride ($BiCl_3$), chromium (III) chloride ($CrCl_3$), nickel (II) chloride ($NiCl_2$), and 1,2-Dichloroethane were purchased from Aladdin. DCE and DMF were purchased from Sinopharm Chemical. PMMA (heat stability injection grade) was purchased from Shanghai Macklin. UV absorber was purchased from Ningbo Xuhong Energy Saving Technology Co. Ltd. ITO glass and double-layer Low-E glass was purchased from Intex Glass (Xiamen) Co. Ltd.

Preparation of the PC Films Doped with Different Ions: A control coater (PF400, Jiangsu LEBO) was used to prepare the PC films. WCl_6 (0.6 g) was dissolved in 3 mL of DMF and different metal-chlorides were added separately, and the molar ratio of the doped metal ions to elemental W was maintained at 40 mol%. The mixture was stirred for 2 h at room temperature to form a solution. PMMA (8 g) was dissolved in 16 mL of DCE for 8 h at room temperature. The two are mixed and stirred for 1 h at room temperature to obtain a precursor solution for the PC films. Then, the coating was applied using a 200 µm gap, which was pushed forward over the mixture automatically by the coater at 70 °C on the glass substrate surface. The speed of the applicator movement was ≈100 mm s^{-1}. And it was placed on the hotplate of the applicator at 70 °C for 30 min to evaporate the solvent. After detaching the coating layer from the substrate, the PC film was obtained.

Preparation of the PC Films Doped with Different Fe Concentrations: Consistent with the above process, except that the weight of $FeCl_3$ was varied to obtain Fe-W-PC membranes with Fe elemental concentrations of 20 mol%, 40 mol%, 60 mol%, 80 mol%, 100 mol%, and 120 mol%, respectively.

Preparation of the DDP Windows with Thermoelectric Devices: A flat panel thermoelectric device with model 03103, having a size of 15 mm × 15 mm × 3.5 mm, was arranged around the glass at 10 mm intervals, with 4 units on each side, totalling 16 units. The wires of each thermoelectric device were connected in series with the high-temperature heat absorbing end facing upward and soldered together. The upper surface of the lower glass is coated by a Low-E film, while the upper surface of the upper glass is covered by the Fe-W-PC film. Thermal conductive silicone grease is used between the device and the glass to fix the thermoelectric devices. The device resistance with no temperature difference at both ends was tested with a multimeter. The devices were placed in sunlight for more than 30 min to achieve a balanced state of the Fe-W-PC film. A KEITHLEY 2401 voltmeter was used for testing the output voltage V_p generated under different output currents I_p.

Characterizations: The transmission, reflection, and absorption spectra of the Fe-W-PC films were recorded at intervals with a spectrometer Cary 7000, Agilent with integrating sphere attachment during the solar simulator (PL-X300DF) illumination (100 mW cm^{-2}) and at intervals during the bleaching process. The process was repeated by varying the intensity of the solar simulator. The light intensity is calibrated by CEL-NP2000-2(10)A, CEAULIGHT. All pictures are obtained by a D7200 Nikon camera. SEM images were obtained by an S-4300. HAADF STEM images were obtained by a JEM-ARM300F.

Energy Performance Calculations: To define the glazing characteristics, the Fe-W-PC film was placed on a single clear glass plate of 2 mm thick. The transmission and reflection measurements were performed after maintaining various sunlight intensities using a PL-X300DF solar simulator for 30 min allowing the film to reach a steady state. This was done upon increasing and decreasing the sunlight intensity to include hysteresis between the steady states during the tinting and bleaching process. The steady-state spectra at a certain sunlight intensity were averaged and implemented in the LBNL software Optics6 to define the optical properties at a certain sunlight intensity. The model office was designed in DesignBuilder according to the previous work.[32,37] During the simulations all modeling parameters are kept constant, except for the glazing. It is designed within DesignBuilder for the Low-E coated double glazing with and without Fe-W-PC film in both summer and winter mode. For the Low-E coated glass plate, the input optical data from Saint-Gobain Eclaz 4 mm were taken from the IGDB database in DesignBuilder. Argon 16 mm was chosen as gas filling between the two glass plates. For the reference case without Fe-W-PC film, the second glass pane was defined by the optical properties of the 2 mm glass plate. For the case with Fe-W-PC film, the second glass pane was defined by the optical properties of the 2 mm glass plate with the Fe-W-PC film in its transparent state as measured. To introduce the photochromic effect in the calculation, the "window shading" feature was used. Here, the optical properties of the second glass pane at various sunlight intensities were defined based on the optical properties determined above. The window shading was controlled by "daylight only" and operates "24/7′ to mimic the autonomous working principle of the Fe-W-PC film. For the model calculation each window was provided with a single light-intensity 'sensor", so the various windows of the building model operate individually. The weather data files were downloaded from www.climate.onebuilding.org, which provides Typical Meteorological Year (TMY) datasets for the specific locations, which were then imported into the DesignBuilder model.

Supporting Information

Supporting Information is available from the Wiley Online Library or from the author.

Acknowledgements

W.M. and A.J.J.K. contributed equally to this work. The authors thank the financial support by the Chinese Academy of Sciences and Dutch research project (1A111KYSB20190072) and the National Natural Science Foundation of China (52373001, 51873221, 52073292, 51673207, 51373183, and 21988102). The authors would also like to acknowledge the funding of this project (482.19.700) by the Netherlands Organization for Scientific Research (NWO), through the Merian Fund, in the framework of the program Green Cities 2019.

Conflict of Interest

The authors declare no conflict of interest.

Data Availability Statement

The data that support the findings of this study are available from the corresponding author upon reasonable request.

Keywords

dual mode, energy saving, photochromic, smart windows, thermoelectric

Received: February 8, 2024
Revised: March 10, 2024
Published online: April 3, 2024

[1] United Nations Environment Programme. 2022 Global Status Report for Buildings and Construction: Towards a Zero-emission, Efficient and Resilient Buildings and Construction Sector. Nairobi, **2022**.
[2] Y. Zhou, F. Fan, Y. P. Liu, S. S. Zhao, Q. Xu, S. C. Wang, D. Luo, Y. Long, *Nano Energy* **2021**, *90*, 106613.
[3] H. Yin, X. Zhou, Z. Zhou, R. Liu, X. Mo, Z. Chen, E. Yang, Z. Huang, H. Li, H. Wu, J. Zhou, Y. Long, B. Hu, *Research* **2023**, *6*, 0103.

[4] H. Khandelwal, A. P. H. J. Schenning, M. G. Debije, *Adv. Energy Mater.* **2017**, *7*, 1602209.
[5] J. Chai, J. Fan, *Adv. Energy Mater.* **2022**, *13*, 2202932.
[6] Y. J. Ke, J. W. Chen, C. J. Lin, S. C. Wang, Y. Zhou, J. Yin, P. S. Lee, Y. Long, *Adv. Energy Mater.* **2019**, *9*, 1902066.
[7] E. Abraham, V. Cherpak, B. Senyuk, J. B. ten Hove, T. Lee, Q. Liu, I. I. Smalyukh, *Nat. Energy* **2023**, *8*, 381.
[8] J. Wang, D. Yuan, P. Hu, Y. Wang, J. Wang, Q. Li, *Adv. Funct. Mater.* **2023**, *33*, 2300441.
[9] Z. Zhou, Y. Fang, X. Wang, E. Yang, R. Liu, X. Zhou, Z. Huang, H. Yin, J. Zhou, B. Hu, *Nano Energy* **2022**, *93*, 106865.
[10] S. C. Wang, Y. Zhou, T. Y. Jiang, R. G. Yang, G. Tan, Y. Long, *Nano Energy* **2021**, *89*, 106440.
[11] S. Z. Sheng, J. L. Wang, B. Zhao, Z. He, X. F. Feng, Q. G. Shang, C. Chen, G. Pei, J. Zhou, J. W. Liu, S. H. Yu, *Nat Commun* **2023**, *14*, 3231.
[12] M. T. Strand, T. S. Hernandez, M. G. Danner, A. L. Yeang, N. Jarvey, C. J. Barile, M. D. McGehee, *Nat. Energy* **2021**, *6*, 546.
[13] Y. Deng, Y. Yang, Y. Xiao, H. L. Xie, R. Lan, L. Zhang, H. Yang, *Adv. Funct. Mater.* **2023**, *33*, 2301319.
[14] Z. Shao, A. Huang, C. Ming, J. Bell, P. Yu, Y. Y. Sun, L. Jin, L. Ma, H. Luo, P. Jin, X. Cao, *Nat. Electron.* **2022**, *5*, 45.
[15] S. Wang, T. Jiang, Y. Meng, R. Yang, G. Tan, Y. Long, *Science* **2021**, *374*, 1501.
[16] X. Li, C. Cao, C. Liu, W. He, K. Wu, Y. Wang, B. Xu, Z. Tian, E. Song, J. Cui, G. Huang, C. Zheng, Z. Di, X. Cao, Y. Mei, *Nat. Commun.* **2022**, *13*, 7819.
[17] C. Lin, J. Hur, C. Y. H. Chao, G. Liu, S. Yao, W. Li, B. Huang, *Sci. Adv.* **2022**, *8*, eabn7359.
[18] J. C. Li, P. Y. Gu, H. Y. Pan, Z. Y. Qiao, J. F. Wang, Y. X. Cao, W. J. Wang, Y. Y. Yang, *Adv. Sci.* **2023**, *10*, 2206044.
[19] G. Chen, K. Wang, J. Yang, J. Huang, Z. Chen, J. Zheng, J. Wang, H. Yang, S. Li, Y. Miao, W. Wang, N. Zhu, X. Jiang, Y. Chen, J. Fu, *Adv. Mater.* **2023**, *35*, 2211716.
[20] Y. Feng, S. Wang, Y. Li, W. Ma, G. Zhang, M. Yang, H. Li, Y. Yang, Y. Long, *Adv. Funct. Mater.* **2023**, *33*, 2211027.
[21] B. Li, F. Xu, T. Guan, Y. Li, J. Sun, *Adv. Mater.* **2023**, *35*, 2211456.
[22] Y. Liu, Y. Zhang, T. Chen, Z. Jin, W. Feng, M. Li, L. Chen, C. Wang, *Adv. Funct. Mater.* **2023**, *33*, 2307240.
[23] W. Meng, Y. Gao, X. Hu, L. Tan, L. Li, G. Zhou, H. Yang, J. Wang, L. Jiang, *ACS Appl. Mater. Interfaces* **2022**, *14*, 28301.
[24] B. A. Rosales, J. Kim, V. M. Wheeler, L. E. Crowe, K. J. Prince, M. Mirzokarimov, T. Daligault, A. Duell, C. A. Wolden, L. T. Schelhas, L. M. Wheeler, *Adv. Energy Mater.* **2023**, *13*, 2203331.
[25] Y. Zhu, Y. J. Yao, Z. Chen, Z. T. Zhang, P. Zhang, Z. F. Cheng, Y. F. Gao, *Sol. Energy Mater. Sol. Cells* **2022**, *239*, 111664.
[26] Y. Badour, S. Danto, S. Albakour, S. Mornet, N. Penin, L. Hirsch, M. Gaudon, *Sol. Energy Mater. Sol. Cells* **2023**, *255*, 112291.
[27] S. Y. Chun, S. Park, S. I. Lee, H. D. Nguyen, K. K. Lee, S. Hong, C. H. Han, M. Cho, H. K. Choi, K. Kwak, *Nano Energy* **2021**, *82*, 105721.
[28] C. W. Kim, E. G. Santoro, A. U. Pawar, D. K. Lee, O. Peña-Rodriguez, U. Pal, Y. S. Kang, *J Ocul Pharmacol Ther* **2022**, *11*, 2202171.
[29] S. Sarwar, S. Park, T. T. Dao, S. Hong, C. H. Han, *Sol. Energy Mater. Sol. Cells* **2021**, *224*, 110990.
[30] Q. Zhang, A. Huang, X. Ai, J. Liao, Q. Song, H. Reith, X. Cao, Y. Fang, G. Schierning, K. Nielsch, S. Bai, L. Chen, *Adv. Energy Mater.* **2021**, *11*, 2101213.
[31] R. Kay, C. Katrycz, K. Nitiema, J. A. Jakubiec, B. D. Hatton, *Nat Commun* **2022**, *13*, 4120.
[32] W. Meng, A. J. J. Kragt, Y. Gao, E. Brembilla, X. Hu, J. S. van der Burgt, A. P. H. J. Schenning, T. Klein, G. Zhou, E. R. van den Ham, L. Tan, L. Li, J. Wang, L. Jiang, *Adv. Mater.* **2023**, *36*, 2304910.
[33] W. Yang, P. Xiao, S. Li, F. Deng, F. Ni, C. Zhang, J. Gu, J. Yang, S. W. Kuo, F. Geng, T. Chen, *Small* **2023**, *19*, 2302509.
[34] S. Tao, J. Han, Y. Xu, Z. Fang, Y. Ni, L. Fang, C. Lu, Z. Xu, *ACS Appl. Mater. Interfaces* **2023**, *15*, 17123.
[35] M. Shi, Z. Song, J. Ni, X. Du, Y. Cao, Y. Yang, W. Wang, J. Wang, *ACS Nano* **2023**, *17*, 2029.
[36] K. C. S. Ly, X. Liu, X. Song, C. Xiao, P. Wang, H. Zhou, T. Fan, *Adv. Funct. Mater.* **2022**, *32*, 2203789.
[37] Y. N. Song, M. Q. Lei, D. L. Han, Y. C. Huang, S. P. Wang, J. Y. Shi, Y. Li, L. Xu, J. Lei, Z. M. Li, *ACS Appl. Mater. Interfaces* **2021**, *13*, 19301.
[38] J. Pu, C. Shen, J. Wang, Y. Zhang, C. Zhang, S. A. Kalogirou, *Nano Energy* **2023**, *110*, 108334.
[39] X. Dong, Y. Lu, X. Liu, L. Zhang, Y. Tong, *J. Photochem. Photobiol., C* **2022**, *53*, 100555.
[40] K. Thummavichai, Y. D. Xia, Y. Q. Zhu, *Prog. Mater. Sci.* **2017**, *88*, 281.